JBC RESEARCH ARTICLE

Dipeptidyl peptidase 4 contributes to Alzheimer's disease–like defects in a mouse model and is increased in sporadic Alzheimer's disease brains

Received for publication, December 13, 2020, and in revised form, June 25, 2021 Published, Papers in Press, July 12, 2021,
https://doi.org/10.1016/j.jbc.2021.100963

Audrey Valverde, Julie Dunys, Thomas Lorivel, Delphine Debayle, Anne-Sophie Gay, Céline Caillava, Mounia Chami, and Frédéric Checler*

From the Team Labeled "Laboratory of Excellence (LABEX) Distalz", INSERM, CNRS, IPMC, Université Côte d'Azur, Sophia-Antipolis, Valbonne, France

Edited by Paul Fraser

The amyloid cascade hypothesis, which proposes a prominent role for full-length amyloid β peptides in Alzheimer's disease, is currently being questioned. In addition to full-length amyloid β peptide, several N-terminally truncated fragments of amyloid β peptide could well contribute to Alzheimer's disease setting and/or progression. Among them, pyroGlu3–amyloid β peptide appears to be one of the main components of early anatomical lesions in Alzheimer's disease–affected brains. Little is known about the proteolytic activities that could account for the N-terminal truncations of full-length amyloid β, but they appear as the rate-limiting enzymes yielding the Glu3–amyloid β peptide sequence that undergoes subsequent cyclization by glutaminyl cyclase, thereby yielding pyroGlu3–amyloid β. Here, we investigated the contribution of dipeptidyl peptidase 4 in Glu3–amyloid β peptide formation and the functional influence of its genetic depletion or pharmacological blockade on spine maturation as well as on pyroGlu3–amyloid β peptide and amyloid β 42–positive plaques and amyloid β 42 load in the triple transgenic Alzheimer's disease mouse model. Furthermore, we examined whether reduction of dipeptidyl peptidase 4 could rescue learning and memory deficits displayed by these mice. Our data establish that dipeptidyl peptidase 4 reduction alleviates anatomical, biochemical, and behavioral Alzheimer's disease–related defects. Furthermore, we demonstrate that dipeptidyl peptidase 4 activity is increased early in sporadic Alzheimer's disease brains. Thus, our data demonstrate that dipeptidyl peptidase 4 participates in pyroGlu3–amyloid β peptide formation and that targeting this peptidase could be considered as an alternative strategy to interfere with Alzheimer's disease progression.

Alzheimer's disease (AD) is the main age-related neurodegenerative disease, the etiology of which remains a matter of questions. One of the main hypotheses referred to as the "amyloid cascade hypothesis" (1) postulates a key role of amyloid β (Aβ) peptide accumulation (2) in various brain zones, including those controlling memory, a psychometric paradigm altered in AD and that worsens as the disease progresses. However, the consistent failure of Aβ-centric clinical trials aimed at reducing Aβ load by immunotherapy or pharmacological targeting of its generating enzyme γ-secretase (3, 4) casts some doubts about the validity of this hypothesis (5). It remains that, undoubtedly, genetic evidence brought a crystal-clear demonstration that amyloid precursor protein (APP)-linked fragments could participate in the pathology. Several APP-linked catabolites distinct from genuine full-length Aβ (flAβ) were shown to account for some of early lesions of AD-affected brains and could well contribute to the pathology (6–11).

Aβ itself is the product of a physiological APP processing (2, 12, 13) and displays physiological/protective functions (14–16) but could be converted into shorter toxic fragments contributing to the pathology (17). Particularly interesting is the pyroGlu3–Aβ (pE3-Aβ) fragment that derives from an N-terminal dipeptide truncation of Aβ yielding a Glu3-Aβ (E3-Aβ) peptide that is subsequently cyclized by glutaminyl cyclase (QC) (18, 19). Numerous anatomical and biochemical evidences suggested that QC is involved in the conversion of E3-Aβ into pE3-Aβ, but the most straightforward demonstration of its key role was brought by studies showing that its pharmacological blockade or genetic depletion alleviates AD-like cognitive defects in an AD mouse model (20).

Dipeptidyl aminopeptidase 4 (DPP4) is an exopeptidase that was formerly described, by fluorogenic dipeptides substrates screening, as an exopeptidase preferentially cleaving X-Pro sequence (21) and hence, was first referred to as a post–proline dipeptidyl aminopeptidase (22). However, it appeared that most of its main natural substrates harbor an N-terminal dipeptide X-Ala. Strikingly, this structural motif corresponds to the N-terminal sequence (Asp-Ala) of the Aβ peptide. Therefore, DPP4 appears as a good enzyme candidate responsible for the rate-limiting removal of this dipeptide. Indeed, few studies showed that DPP4 could, in concert with QC, yield pE3-40/42Aβ, *in vitro* (23) and that DPP4 inhibitors could prove useful as an AD treatment (24, 25).

Here, we show by MS that human recombinant DPP4 releases the N-terminal dipeptide of synthetic Aβ40 and in agreement, that a DPP4 specific inhibitor potentiates the recovery of flAβ generated by APP-expressing human cells. We show that the pharmacological blockade of DPP4 by its specific

* For correspondence: Frédéric Checler, checler@ipmc.cnrs.fr.
Present address for Céline Caillava: Genbiotech, Antibes, France.

inhibitor sitagliptin rescues dendrite morphological alterations in organotypic slices derived from mice infected with lentiviruses harboring the APP bearing the Swedish mutation (APPswe) sequence. Furthermore, both sitagliptin and shRNA directed toward DPP4 reduce the number of Aβ42-positive plaques and Aβ40/42 loads in triple transgenic AD (3xTg-AD) mouse brain. We also establish that DPP4 genetic reduction and/or sitagliptin alleviate cognitive defects assessed by the Morris water maze (MWM) and Barnes maze tests in 3xTg-AD mice. Finally, we document a Braak stage–dependent and transient augmentation of DPP4 activity in a cohort of sporadic AD brains. Altogether, our data bring novel insights supporting the possibility that DPP4 could contribute to AD pathology.

Results

Pharmacological blockade of DPP4 potentiates Aβ full-length recovery in cells

By using antibodies that interact only with the free N-terminal aspartyl residue of Aβ (FCA18, (26)), we previously established that aminopeptidase A (APA) inhibitors potentiate the recovery of flAβ generated by human cells overexpressing APPswe (14). Here, we show as a control that, as expected, flAβ recovery was highly enhanced when neprilysin, one of the main Aβ-degrading enzymes (27, 28), was blocked with its highly specific and potent inhibitor phosphoramidon (Fig. 1). Furthermore, we assessed the potential effect of the aminopeptidase M (PL250) (29), APA (PL302) (30), and DPP4 (P32/98) inhibitors (31). PL302 and P32/98 but not PL250 significantly potentiated the recovery of flAβ (Fig. 1). Interestingly, we observed an additive effect of PL302 and P32/98 (Fig. 1). These data indicate that APA and DPP4 but not aminopeptidase M contribute to the N-terminal truncation of flAβ and that these catalytic events are likely independent.

DPP4 removes the N-terminal dipeptide of Aβ40-An MS approach

We analyzed the capability of human recombinant DPP4 (rDPP4) to generate Aβ3-40 from synthetic Aβ40. By MS analysis, we found that DPP4 converts Aβ1-40 synthetic peptide into Aβ3-40, thus releasing the N-terminal dipeptide of Aβ40 (Fig. 2, *A* and *B*). Importantly, the Aβ3-40/Aβ1-40 ratio

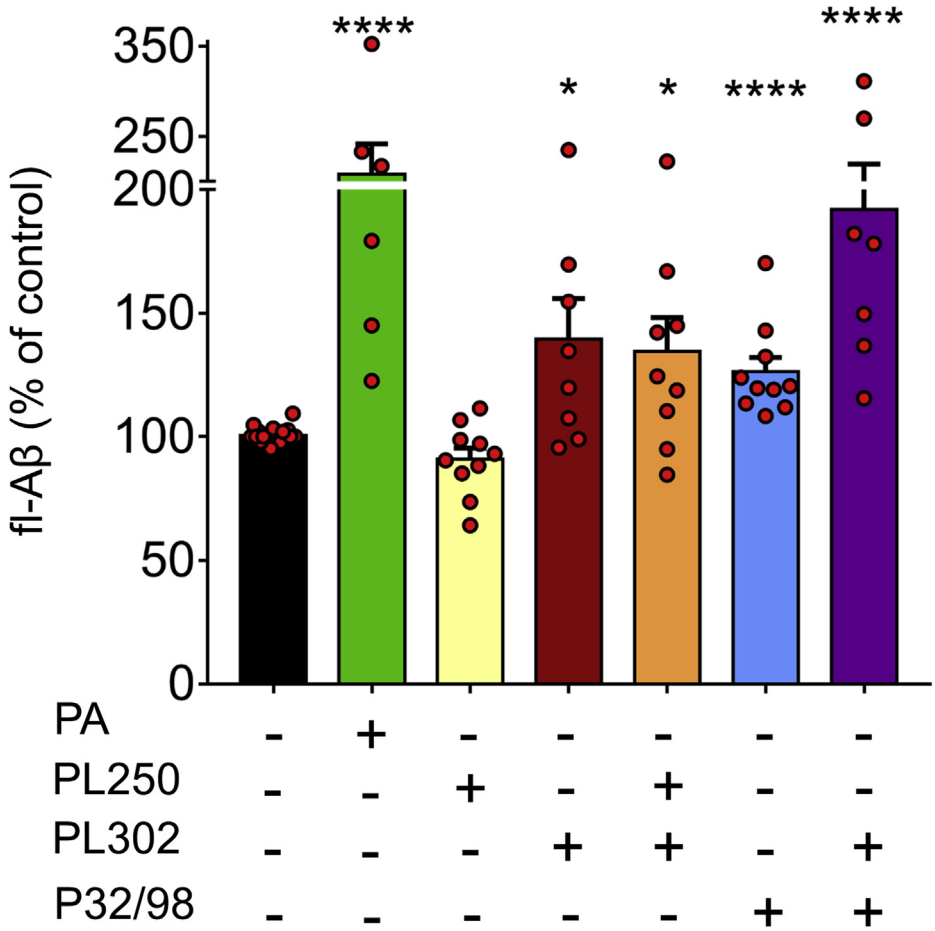

Figure 1. Effects of pharmacological modulation of endogenous DPP4 in HEK APPwt cells on full-length Aβ expression. Full-length Aβ immunoreactivity in HEK APPwt cells treated without (control) or with phosphoramidon (PA), PL302, PL250, and P32/98 (aminopeptidase A, aminopeptidase M, and DPP4 inhibitors, respectively) was quantitated by densitometry. Values are expressed as the percentage of control untreated cells (taken as 100) and are the means ± SEM of 6 to 17 determinations obtained from seven independent experiments. *$p < 0.05$ and ****$p < 0.0001$ (Mann–Whitney test). Aβ, amyloid β; APPwt, WT APP; DPP4, dipeptidyl aminopeptidase 4; flAβ, full-length Aβ; HEK, human embryonic kidney.

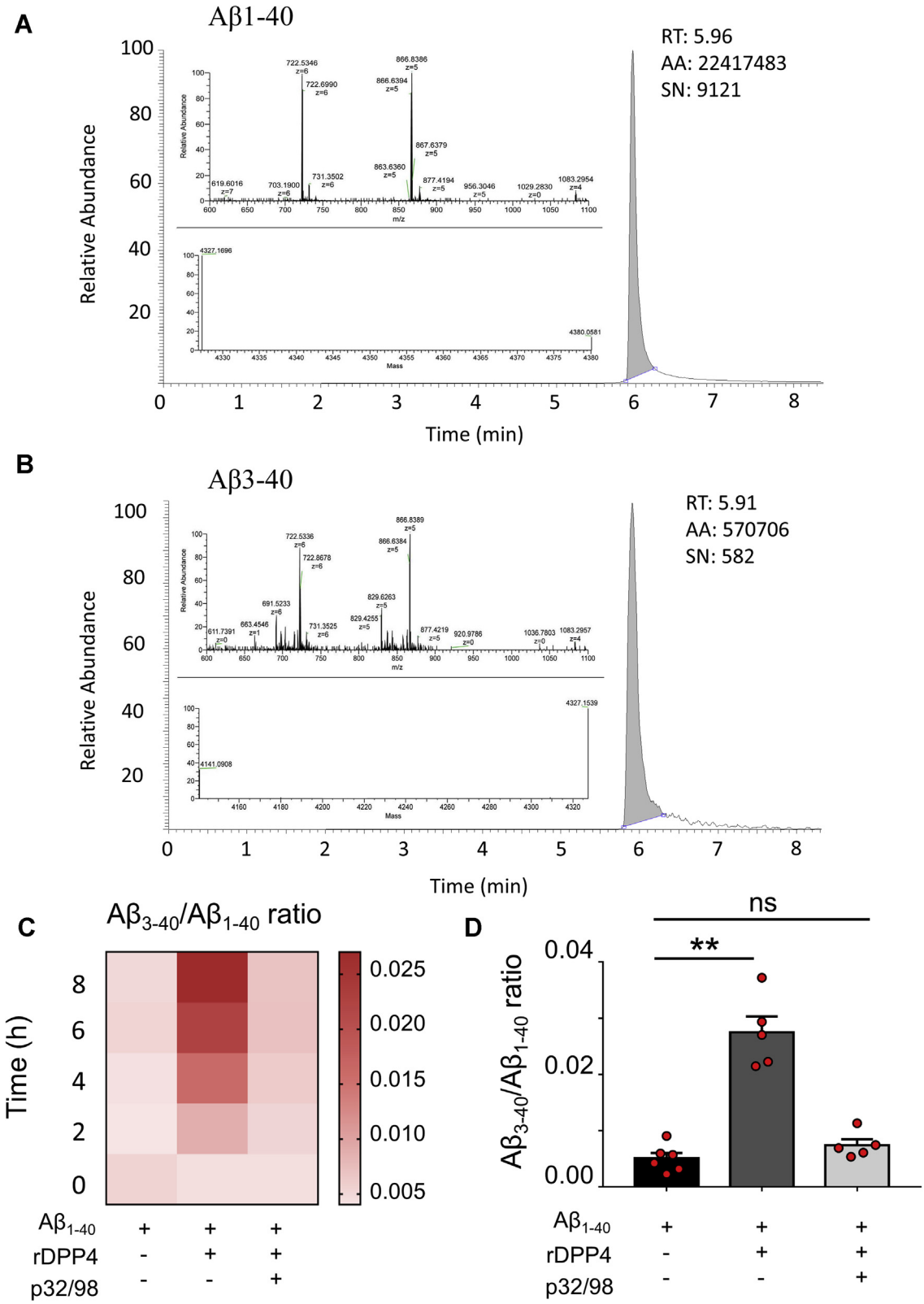

Figure 2. DPP4 releases the N-terminal dipeptide of Aβ40. HPLC chromatograms of Aβ1-40 (*A*) and Aβ3-40 (*B*) peptides and their spectral deconvolution revealing m/z values (4327.1515 and 4141.0908, respectively) recovered after a 6-h incubation of human recombinant DPP4 with synthetic Aβ40. *C*, Aβ3-40/Aβ1-40 ratio is represented over time in presence or absence of rDPP4, with or without p32/98 inhibitor. *D*, quantification of Aβ3-40/Aβ1-40 ratio observed after 8 h. Values are the means ± SEM of 5 to 6 determinations obtained from three independent experiments. (**$p < 0.01$; one-way ANOVA with Dunn's multiple comparisons post-test). Aβ, amyloid β; AA, average area; DPP4, dipeptidyl aminopeptidase 4; ns, not statistically significant; RT, retention time; SN, signal noise.

increased with time and was prevented by the DPP4-specific inhibitor p32/98 (31) (Fig. 2, *C* and *D*).

DPP4 inhibition rescues alterations of dendritic spine morphology

We have evaluated the putative impact of DPP4 on spine morphology of hippocampal organotypic slices infected with lentiviruses expressing green, WT APP, or APPswe-green constructs (see expressions in Fig. 3*B*, upper panels). The spine morphology (Fig. 3*B*, lower panels) was classified within three categories: mature (mushroom/thin, Fig. 3*C*, red bars), stubby (Fig. 3*C*, yellow bars), and immature spines (filopodia, Fig. 3*C*, green bars). First, of note, the expression of the various constructs did not affect neuronal viability as assessed by NeuN expression (Fig. S1). APPswe-expressing slices show a lower number of mature spines than WT APP (APPwt) and green, and a concomitant increase of dendritic filopodia (compare APPwt NT and APPswe NT conditions in Fig. 3*C*). Of importance, the morphological alterations observed in APPswe-expressing slices were fully rescued by pretreatment with the highly potent and selective DPP4 inhibitor sitagliptin (32), (Fig. 3, *B* and *C*, compare APPswe NT *versus* Sita). This suggested the possibility that DPP4-mediated sitagliptin-sensitive production of pE3-Aβ could account for the alteration of dendritic spines in these organotypic slices. To support this view, we checked whether organotypic slices harbor functional DPP4 and if they produce pE3-Aβ. Our data show that indeed, organotypic slices express pE3-Aβ-like *in situ* immunoreactivity (Fig. S2*A*) that is present in insoluble fractions prepared from these slices (Fig. S2*B*) and display sitagliptin-sensitive DPP4-hydrolyzing activity (Fig. S2*C*). It is of importance to note that our recent study indicated that synthetic pE3-Aβ could indeed alter dendritic morphology and mimic that triggered by APPswe expression (33). Overall, this set of data indicates that DPP4 contributes to the morphological alterations affecting spines in an *ex vivo* AD model.

Genetic reduction and pharmacological blockade of DPP4 reduce pE3-42Aβ and Aβ plaque loads

We attempted to reduce DPP4 expression and activity by shRNA approach. We designed several shRNA probes targeting DPP4 (shDPP4) as well as an shRNA corresponding to a control scramble sequence (shScr). We first examined their ability to lower DPP4 expression and activity in N2a cells. Among them, one sequence (see Experimental procedures) was selected because its transfection reduced the number of DPP4-positive N2a cells by about 30% when compared with shScr (Fig. S3, *A* and *B*). Then, we produced lentiviruses harboring the shScr and shDPP4 sequences coupled with GFP. This allowed to confirm that stereotaxical delivery of shRNAs adequately yielded GFP expression in the subiculum of the hippocampus of mouse brains (Fig. S3*C*). shDPP4 infection triggers an about 25% reduction of DPP4 activity in WT mouse brain (Fig. S3, *D* and *E*).

We have examined the biochemical and anatomical impacts of DPP4 gene reduction in 3xTg-AD mice infected or not at the age of 3 months with the above-selected shDPP4- or shScr-expressing lentiviruses. At the age of 12 months, DPP4 downregulation drastically reduces the number of Aβ42-positive plaques (Fig. 4, *A* and *B*) without affecting their mean perimeter (Fig. 4*C*) and areas (Fig. 4*D*). Interestingly, we also observed a decreased expression of pE3-Aβ in 3xTg-AD mice infected with shDPP4 (Fig. S4). Accordingly, as expected at this age, both Aβ40 and Aβ42 recoveries were much higher in the insoluble fraction (which mostly contains Aβ in an aggregated state) prepared from shScr-3xTg-AD than in shScr-WT infected mice (Fig. 4, *E* and *F*). However, both Aβ species were drastically lowered in these insoluble fractions upon shDPP4 infection (Fig. 4, *E* and *F*).

We attempted to examine the influence of chronic treatment with sitagliptin. At first, we aimed at assessing whether intraperitoneal administration of sitagliptin could significantly inhibit cerebral DPP4. Indeed, we show that an 8-day treatment of 3-month-old 3xTg-AD mice triggers a reduction of about 30% of cerebral DPP4 activity (Fig. S5). Of note, the extent of sitagliptin-mediated inhibition of central DPP4 was similar to the one achieved by shDPP4 (Fig. S3, *D* and *E*). Although partial, this inhibition could however reflect full blockade of DPP4. Thus, we previously established that Gly-Pro–7-amido-4-methylcoumarin undergoes DPP4-unrelated cleavages in crude tissues (34) that could account for shDPP4 and sitagliptin-resistant hydrolyzing activity. This was performed at an earlier age, when Aβ42-positive plaques are clearly less numerous than at the age of 12 months. Thus, the quantification of the number of plaques was more difficult and suffers from higher randomness. Nevertheless, although it did not reach statistical significance, we observed a consistent reduction of Aβ42-positives plaques (Fig. 5, *A* and *B*), mean area (Fig. 5*C*) and perimeter (Fig. 5*D*). In agreement with a genuine reduction of plaques number, Aβ42 was recovered in a lower amount in the insoluble fraction prepared from sitagliptin-treated 3xTg-AD mice (Fig. 5*F*), while Aβ40 lowering did not reach statistical significance (Fig. 5*E*). Overall, our combined genetic and pharmacological approaches indicate that DPP4 downregulation lowers Aβ-positive plaque formation and Aβ aggregation in 3xTg-AD mice.

Genetic and pharmacological reduction of DPP4 partly alleviates learning and memory defects in 3xTg-AD mice

To determine whether DPP4 activity could modulate memory and learning *in vivo*, we used the 3xTg-AD mouse model that gathers several hallmarks of AD pathology, that are, senile plaques, neurofibrillary tangles, memory deficit, and synaptic plasticity defects (35). We used two well-known spatial learning tests, the MWM and Barnes maze, that are considered as sensitive means to detect memory deficits in these mice (36), to examine the influence of genetic and pharmacological reduction of DPP4 activity. As expected, 3xTg-AD mice were affected in their learning ability as reflected by a higher latency to reach the platform than WT mice in the MWM (Fig. 6*A*). Interestingly, shDPP4 partly rescues these alterations (Fig. 6*A*). This is further supported by the randomness in the trajectories of shScr-treated 3xTg-AD mice (Fig. 6*B*, left panel) that was corrected in shDPP4-treated mice

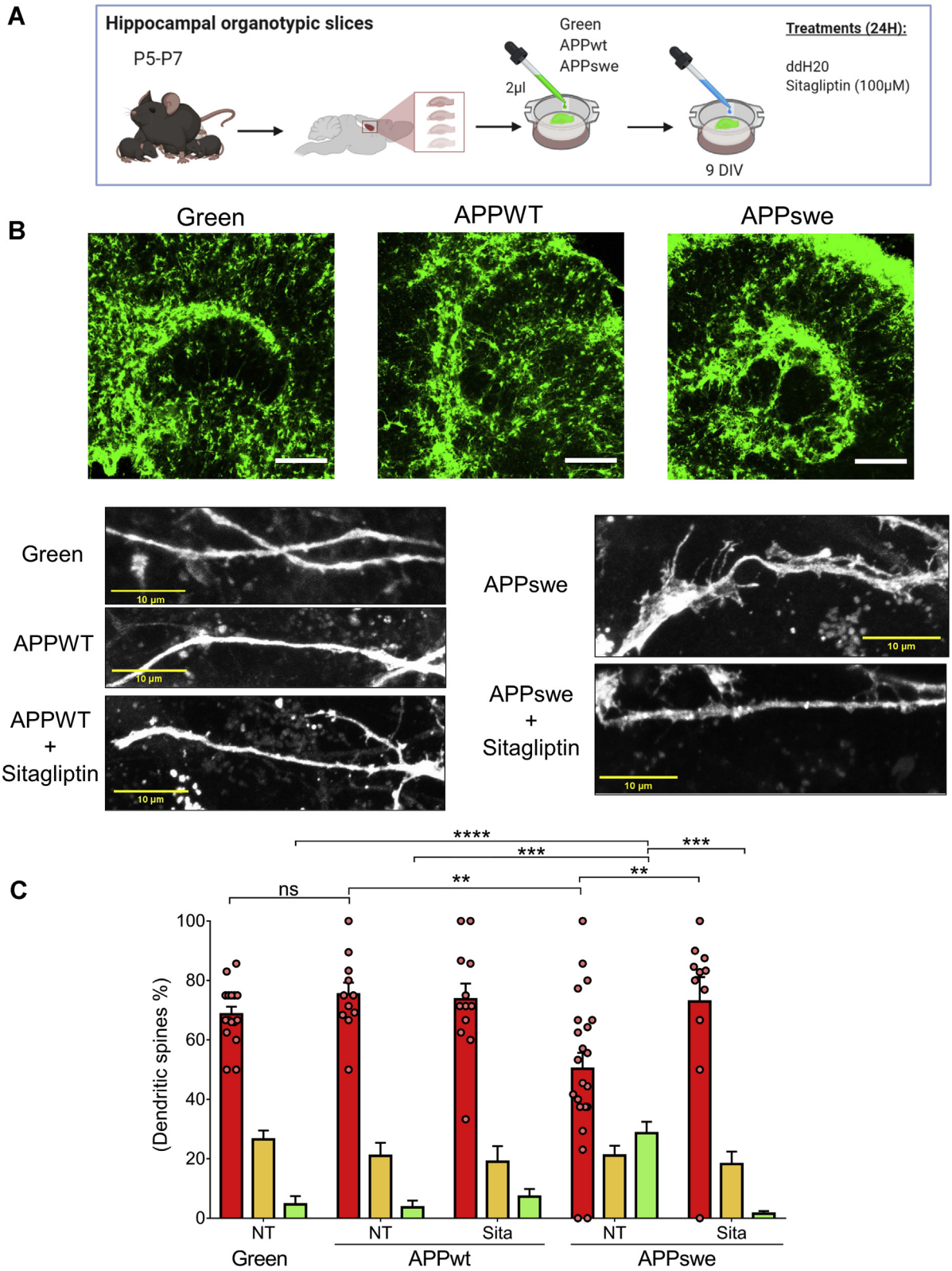

Figure 3. DPP4 pharmacological blockade influences synaptic morphology. Organotypic slices (see procedure in panel *A*) were infected with green (*B*, *left panel*), APPwt (*B*, *middle panel*), or APPswe (*B*, *right panel*) lentivirus coexpressing green protein (*B*) treated or not for 24 h with sitagliptin (100 µM). *C*, graph represents the percentage of spines corresponding to mushroom (*red bars*), stubby (*yellow bars*), and immature (filopodia, *green bars*) categories and are the means ± SEM of 10 to 22 determinations obtained from two independent experiments. $^{**}p < 0.01$, $^{***}p < 0.005$, $^{****}p < 0.0001$, (the Kruskal–Wallis test with Dunn's multiple comparisons post-test). Scale bars in *B upper panels* correspond to 300 µm. APPswe, APP bearing the Swedish mutation; APPwt, WT APP; DPP4, dipeptidyl aminopeptidase 4; ns, not statistically significant.

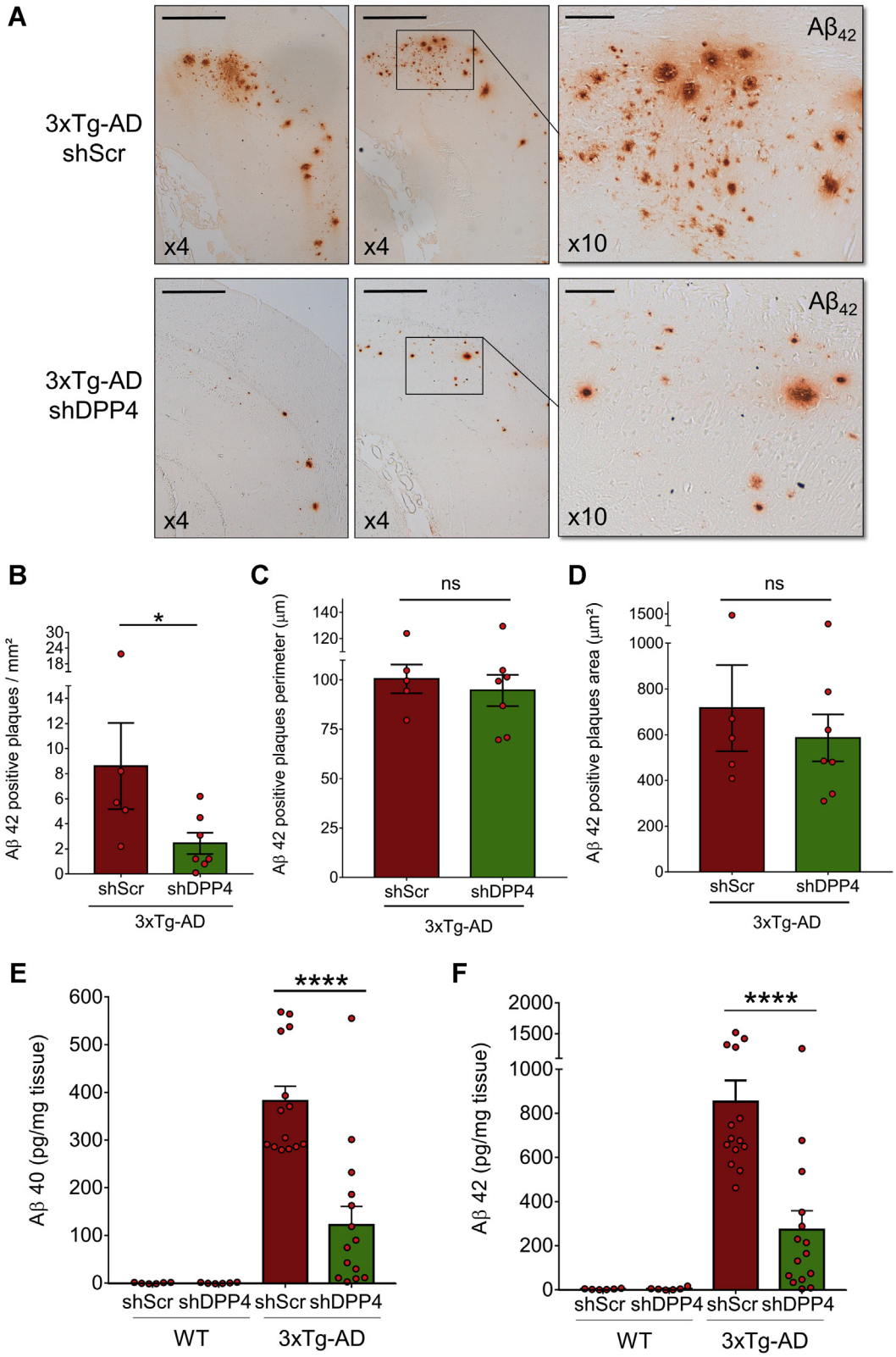

Figure 4. Aβ42-positive plaques and Aβ load are decreased in 3xTg-AD mouse brain after shRNA-mediated reduction of endogenous DPP4. *A*, immunohistochemical analysis using the anti-Aβ42 antibody in 12-month-old 3xTg-AD mice infected with lentiviruses bearing either shScr or shDPP4. Scale bars in panel *A* correspond to 500 µm (4×) or 100 µm (10×). *B*, graph represents the number of Aβ42-positive plaques per square millimeters. *C* and *D*, graphs represent the mean perimeter (*C*) and area (*D*) of Aβ42-positive plaques. *B–D*, data are the means ± SEM of 5 (shScr) or 7 (shDPP4)-injected mice (Mann–Whitney test). *$p < 0.05$. Aβ40 (*E*) and Aβ42 (*F*) measured by ELISA in insoluble fractions prepared from 12-month-old 3xTgWT and 3xTg-AD transgenic mice infected with shScr or shDPP4 lentiviruses as in panel *A*. Values are the means ± SEM of 6 (WTshScr and WtshDPP4) or 14 to 15 (shScr- and shDPP4-injected 3xTg-AD) determinations obtained from two independent experiments and are expressed in pg per mg of tissue. ****$p < 0.0001$ (Mann–Whitney test). 3xTg-AD, triple transgenic AD; Aβ, amyloid β; AD, Alzheimer's disease; DPP4, dipeptidyl aminopeptidase 4; shDPP4, shRNA probes targeting DPP4; shScr, shRNA corresponding to a control scramble sequence.

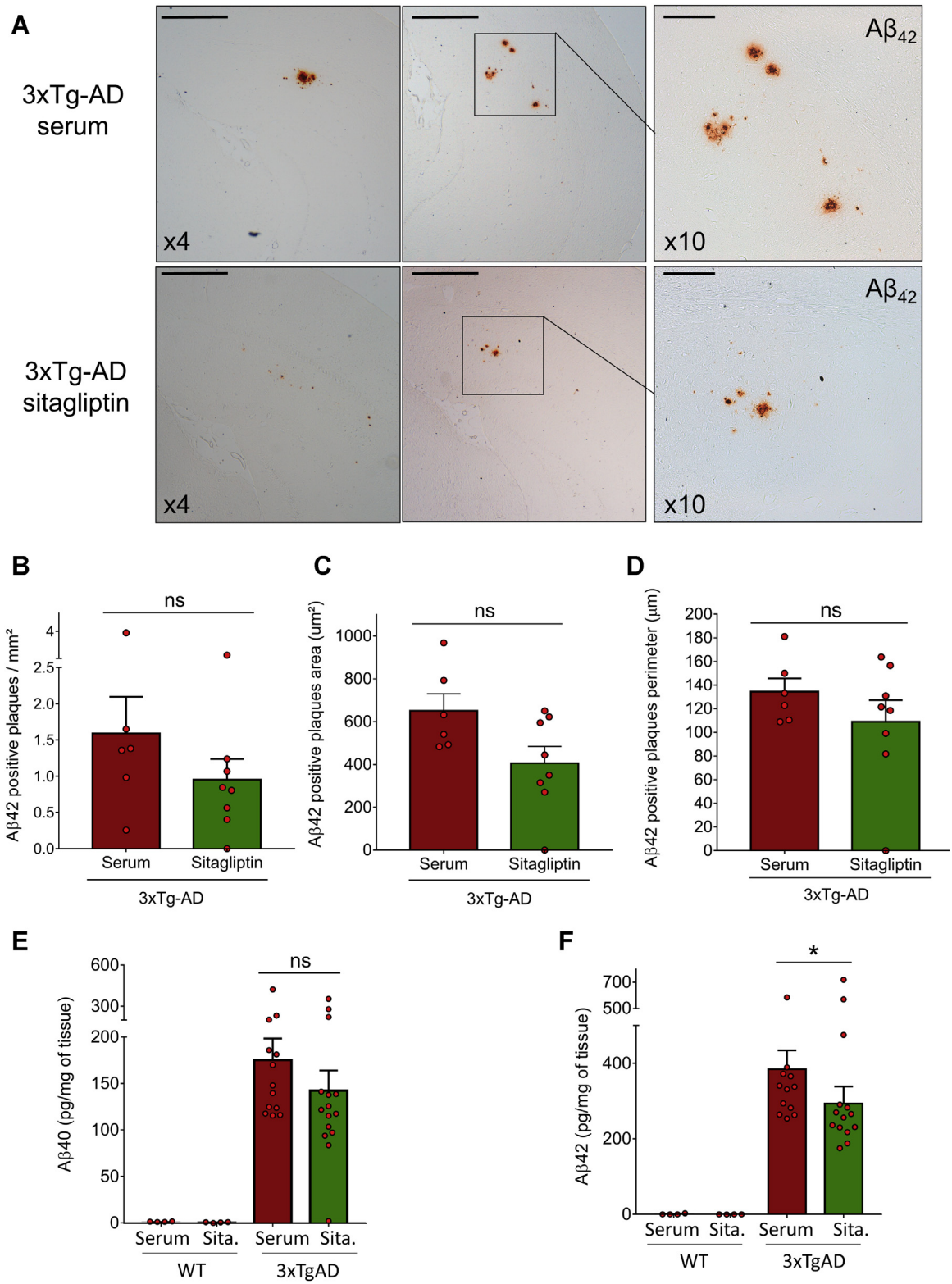

Figure 5. Influence of sitagliptin on Aβ42-positive plaques. *A*, immunohistochemical analysis using anti-Aβ42 antibody in 10- to 11-month-old 3xTg-AD mice chronically treated or not with sitagliptin. Scale bars in panel *A* correspond to 500 µm (4×) or 100 µm (10×). *B*, graph represents the number of Aβ42-positive plaques per square millimeters. Panels *C* and *D* represent the mean area (*C*) and perimeter (*D*) of Aβ42-positive plaques. *B–D*, data are the means ± SEM of 6 (control, physiological serum) or 8 (sitagliptin)-treated mice (Mann-Whitney test). Note that although there is a clear apparent reduction of the number of Aβ42-positive plaques, statistical analysis did not reach significance (Mann–Whitney test). Aβ40 (*E*) and Aβ42 (*F*) measured by ELISA in insoluble fractions prepared from 10- to 11-month-old WT and 3xTg-AD mice chronically treated with sitagliptin as described in Experimental procedures. Values are means of 4 (WT serum and WT sitagliptin) or 13 to 15 (3xTg-AD serum and 3xTg-AD sitagliptin) determinations obtained from two independent experiments and are expressed in pg of Aβ40/42 per mg of proteins. *$p < 0.05$; Mann–Whitney test. 3xTg-AD, triple transgenic AD; Aβ, amyloid β; AD, Alzheimer's disease; ns, not statistically significant.

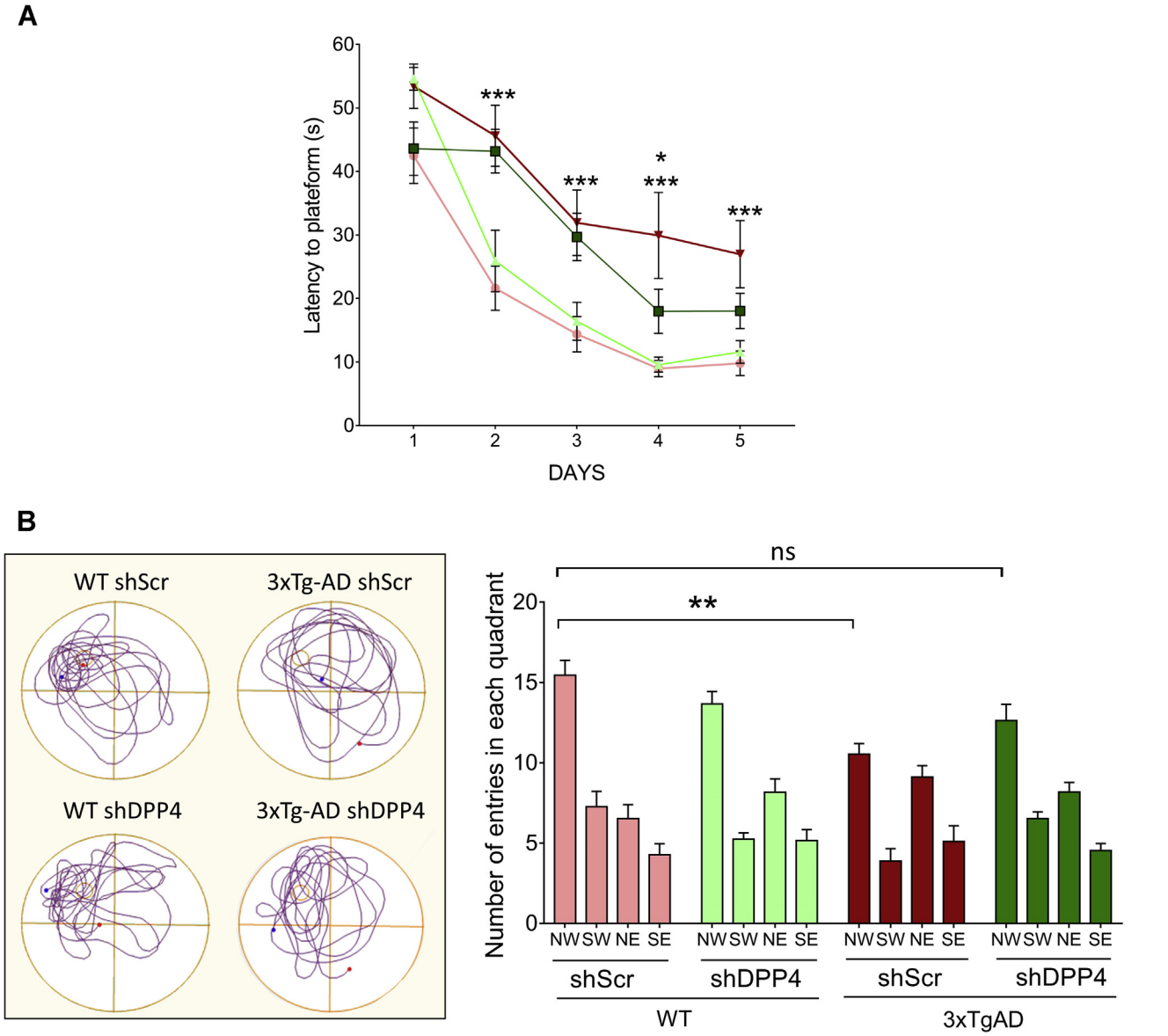

Figure 6. shDPP4 treatment partly restores learning and memory deficits in 3xTg-AD mouse model. *A, graphical* representation of the latency to reach the platform in Morris water maze for 3xTgWT (*light green* and *red curves*) and 3xTg-AD (*dark green* and *red curves*) mice infected with lentiviruses expressing shScr (*light* and *dark red curves*) or shDPP4 (*light* and *dark green curves*). *B*, swimming trajectories of indicated treated mice. Panel *C* shows the number of entries in each quadrant of the Morris water maze. (WT shScr: n = 11; WT shDPP4: n = 12; 3xTg-AD shScr: n = 9; 3xTg-AD shDPP4: n = 11). *$p < 0.05$; **$p < 0.01$; ***$p < 0.005$ (InVivoStat test). 3xTg-AD, triple transgenic AD; AD, Alzheimer's disease; DPP4, dipeptidyl aminopeptidase 4; NE, north east; NW, north west; SE, south east; shDPP4, shRNA probes targeting DPP4; SW, south west.

in probe tests performed at 48 h where treated mice swim in the adequate north west zone virtually similar to WT mice (Fig. 6*B*, right panel). Of note, chronic treatment with sitagliptin indicated that pharmacological blockade of DPP4 also partly rescued the latency to reach the target zone in the Barnes test, a paradigm that was drastically altered in shScr-treated 3xTg-AD mice (Fig. S6*A*). Accordingly, sitagliptin partly improved the distribution of the number of entries in every hole in sitagliptin-treated 3xTg-AD mice (Fig. S6*B*). Of importance, neither sitagliptin nor shDPP4 (data not shown) affects locomotor activity or anxiety parameters as measured by the rotarod and open field test (Fig. S7).

DPP4 activity is increased in brains of patients with AD

It has already been described that pE3-42Aβ is present in abundance in brains of patients with sporadic and familial AD (37). Thus, according to our data, we assumed that there should be an enhanced activity of DPP4 in AD-affected brains. Here, we compared DPP4 activity in hippocampi of controls and patients suffering from sporadic AD at different Braak stages (Table S1). We observed a higher inhibitor-sensitive DPP4 activity in AD brains than in control patients. This increase appears to be AD Braak stage-dependent, culminated at stages I-III and then declined to return to control values at later stages (Fig. 7).

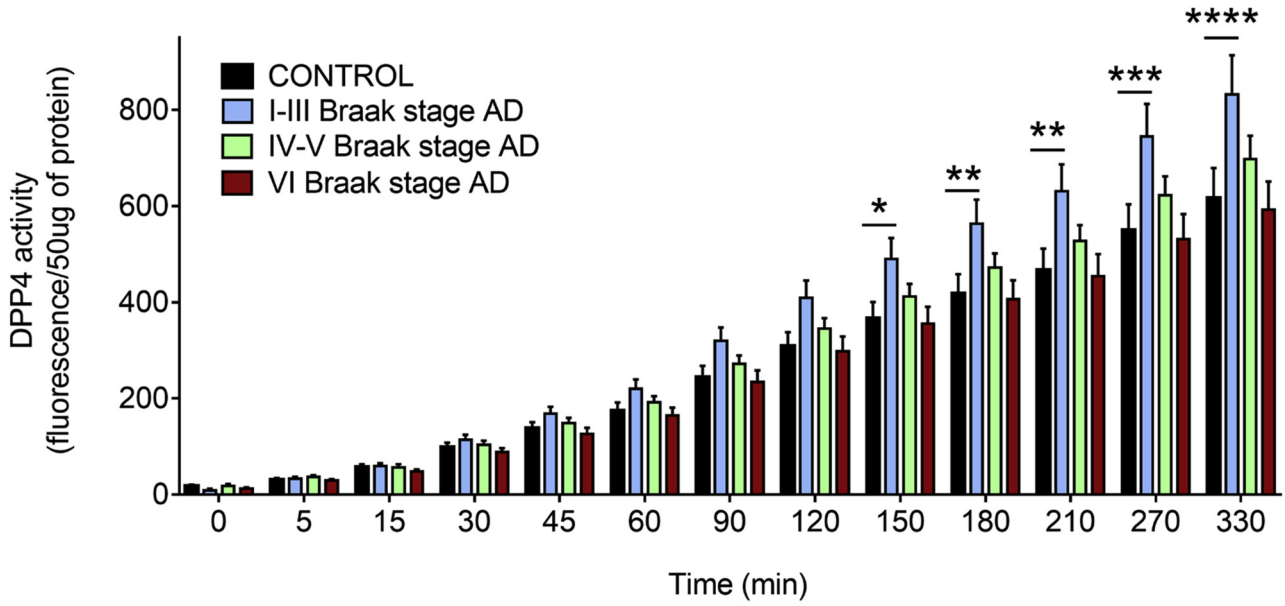

Figure 7. DPP4 enzymatic activity is transiently increased in sporadic AD-affected brains. DPP4 enzymatic activity was measured by fluorimetry as described in Experimental procedures in human brain samples from different Braak stages patients (see Table S1) (controls: n = 10; AD I-III: n = 9; AD IV-V, n = 10; AD VI: n = 14; *$p < 0.05$, **$p < 0.01$, ***$p < 0.0005$, and ****$p < 0.0001$). (Two-way ANOVA test with Dunnett's multiple comparisons test). AD, Alzheimer's disease; DPP4, dipeptidyl aminopeptidase 4.

Discussion

The main conclusion of our study is that the reduction of DPP4 could be beneficial in the context of AD. It is supported by five lines of independent *in vitro*, *ex vivo*, and *in vivo* evidence. First, recombinant DPP4 releases the N-terminal dipeptide of synthetic Aβ. Second, inhibition of DPP4 in human cells potentiates the recovery of secreted flAβ. Third, in APPswe-expressing neurons that display drastic alterations of dendritic spines morphology, pharmacological blockade of DPP4 fully restores a normal phenotype. Fourth, both genetic and pharmacological approaches drastically reduce Aβ42-positive plaques and Aβ40/42 load in insoluble fractions prepared from 3xTg-AD brains. Fifth, shDPP4 and sitagliptin partly rescue learning and memory deficits. Overall, this consistent network of evidence strongly suggests that DPP4 could contribute to the generation of E3-Aβ in AD. It should be noted that DPP4 was documented as the rate-limiting enzyme yielding E3-Aβ amenable to cyclization by QC. These concerted enzymatic events have been previously documented *in vitro* (23).

DPP4 inhibitors have been proposed as means to interfere with cognitive disorders (25). Most of studies deal with type 2 diabetes, a well-recognized risk factor for cognitive dysfunctions and dementia (38). This is mainly due to the propensity of DPP4 to hydrolyze many substrates (39) including GLP-1 (40, 41). GLP-1 is a 30-amino acid peptide which harbors an His-Ala N-terminal dipeptide that fulfills the requirement of DPP4 specificity. Indeed, GLP-1 is one of the preferred substrates of DPP4 (42). Interestingly, although GLP-1 is mainly produced in the intestinal tract, it is also present in the brain and more particularly in the hippocampus and frontal cortex (43). Of note, GLP-1 expression is decreased in patients with AD as well as in AD mouse brain (41). Furthermore, it has been shown that GLP-1 overexpression triggers protective effects and that its DPP4-mediated proteolysis drastically shortens its lifetime (40, 41). Accordingly, DPP4 inhibition favors GLP-1 signaling and improves AD-like cognitive deficits in several AD mouse models (39–41) including the 3xTg-AD mice (41). Our data indicate that, besides GLP-1, DPP4 could also participate to AD pathology by targeting Aβ.

In AD mouse models, several anatomical and functional paradigms including apathy-like phenotype, long term potentiation perturbation, and endolysosomal dysfunction (9, 44, 45) have been shown to occur early and independently of Aβ (7, 46) and, for some of them, are drastically potentiated by γ-secretase inhibitors (7). Recent evidence indicates that the β-secretase-derived fragment of APP (namely C99) could account for these dysfunctions (11). However, at late stage of AD-like pathology, an Aβ-linked contribution to learning and memory defects was observed. The firm demonstration of this Aβ-linked counterpart was brought by the comparison of 3xTg-AD and 2xTg-AD mice (46). The latter mice display similar accumulation of C99 but, unlike 3xTg-AD, they never produce detectable amounts of Aβ (due to the absence of PS1 mutation (46)). Of note, although 3xTg-AD and 2xTg-AD mice display similar early perturbations, the former mice exhibit higher learning and memory defects. Our data indicate that these Aβ-linked alterations of behavior could be accounted for by pE3-Aβ peptides. Of importance, we show that both genetic reduction and pharmacological blockade of DPP4 drastically reduce Aβ42-positive plaques and Aβ42 recovery. This is likely due to the reduction of pE3-Aβ. Thus, it has been shown that very low amounts of pE3-42Aβ are sufficient to serve as Aβ42 seed (47), accelerate its aggregation (23), and thereby, the occurrence of plaques.

It should be emphasized that cognitive alterations are not fully rescued by genetic or pharmacological downregulation of DPP4. This could be explained by the fact that shRNA DPP4 triggers only a partial reduction of the enzyme activity (see Fig. S1) but not by a poor sitagliptin bioavailability after gavage administration (48). Another likely possibility is that besides DPP4, other activities involved in Aβ truncation could occur. One such candidate could be the exopeptidase APA. Thus, this enzyme displays a high affinity for acidic residues such as the N-terminal aspartyl residue of Aβ (22). This hypothesis is supported by our previous study (14) (and present Fig. 2) showing that APA inhibitors enhanced the recovery of cellular flAβ. Furthermore, our recent work showed that the APA inhibitor RB150 and short hairpinRNA directed towards APA both rescue dendritic morphology, lower pE3-Aβ–positive and Aβ-positive plaques and loads, and improve memory defects in 3xTgAD mice (33). Interestingly, APA and DPP4 inhibitor–induced potentiation of flAβ recovery was additive, indicating that the two enzymes independently target flAβ. Thus, the shRNA DPP4-resistant cognitive alterations could be due to residual bioactive DPP4 and APA. It should be noted that we have recently shown that the reduction of APA *in vivo* partly alleviates memory deficits in 3xTg-AD mice (data not shown).

DPP4 is increased in sporadic AD-affected brain, but this increase occurs relatively early at Braak stages I-III and returned to virtually control values at later stages. These data agree well with previous studies showing that DPP4 is upregulated in AD brain neurons and is associated with plaques (49) but not at the late demented stage in both frontal and parietal cortices of patients with AD (50). The increase of DPP4 indeed coincides with the appearance of plaques (our unpublished data), and hence, one can envision that the pE3-Aβ generated could well initiate the seeding of Aβ, its aggregation and the occurrence of plaques. This fits well with the observation that only very low amounts of pE3-42Aβ could serve as a seed of Aβ42 aggregation and deposition (47) and that low amounts of pE3-42Aβ are sufficient to induce hippocampal neurodegeneration in transgenic mice (51). Thus, DPP4 transient increase could be sufficient to initiate a vicious cycle by which AD anatomical lesions progress.

Experimental procedures

MS

Synthetic Aβ40 from Bachem (15 ng/μl) was incubated for various time periods with human recombinant DPP4 (2 ng/μl) (R&D System) or for 6 h with or without the DPP4 inhibitor p32/98 (100 μM). Reactions were stopped after addition of formic acid (0.1%) and then samples were subjected to spectrometry analysis. Briefly, Aβ peptides were separated with UPLC system (Thermo Fisher) on a C18 column in an appropriate gradient. MS data were acquired with a Q-Exactive plus mass spectrometer (Thermo Fisher) operating in the full-scan mode. Finally, Aβ fragments were identified using Xcalibur Quan Browser software (version 4.1.31.9).

Immunoprecipitation procedure

APPwt-overexpressing human embryonic kidney 293 cells were grown in Dulbecco's modified Eagle's medium (DMEM)–fetal calf serum (FCS) (10%)–penicillin/streptomycin medium. Cells were plated in 6-well dishes and allowed to secrete for 8 h in Opti-MEM/FCS (1%) containing phosphoramidon (10 μM) to prevent Aβ degradation by neprilysin (28, 52), with or without aminopeptidase M (pl250), APA (pl302), and DPP4 (p32/98) inhibitors at 5 μM. After media centrifugation, supernatants were completed with one-tenth of RIPA buffer (Tris 50 mM; pH 7.4, containing NaCl (150 mM), EDTA (1 mM), Triton X100 (1%), deoxycholate (0.5%), and SDS (0.1%)) and incubated overnight with a 100-fold dilution of FCA18 antibody (26) and protein A agarose beads (VWR). Beads were washed twice with RIPA buffer 1× and once with Tris (10 mM, pH 7.5) and subjected to Tris/tricine 16.5% polyacrylamide gels. Proteins were transferred onto nitrocellulose and incubated overnight with the 2H3 monoclonal antibody (anti-Aβ1-12 provided by Dr D. Schenk, San Francisco, CA) at a 1/1000 dilution. After secondary antibody incubation with a goat anti-mouse peroxidase-conjugated antibody (1/2000 dilution), chemiluminescence was recorded using LAS-3000 (Raytest) and quantifications were performed using the Multi Gauge software.

Organotypic hippocampal slice preparations and culture

Organotypic hippocampal slices were prepared from 5- to 7-day-old C57bl6JRj mice (Janvier Labs). Brains were quickly dissected to retrieve hippocampi, and then, both hemispheres were sliced in 400-μm sections and kept into the slicing medium (97.5% Earles' Balanced Salt solution (EBSS) and 2.5% EBSS-Hepes). Slices were transferred on sterile hydrophilic membrane Millicell discs (FHLC01300, Millipore) placed in semi-porous cell culture inserts (0.4 μm, Millipore) containing the culture medium (Minimum Essential Medium Eagle + Glutamax-1 (50%), EBSS (18%), EBSS/D-glucose 13% (5%), penicillin-streptomycin (5000 U/ml, 1%), horse serum (25%), and nystatin (10,000 U/ml, 0.06%)). Two hours after plating, slices were infected with lentiviruses encoding for green, APPwt, and APPswe proteins, respectively. Slices were kept at 37 °C, with CO_2 (5%) for 9 days before imaging analysis. For sitagliptin treatment, slices were incubated for 24 h at a concentration of 100 μM.

Imaging of dendrites and quantitation of spine morphology

Slices were left attached on the Millicell membrane and mounted with the mounting solution, cover-slipped, and dried before imaging. Spine morphology was assessed on an average of 14 different dendrite segments (obtained from two independent experiments) taken with Plan-Apochromat 63×/1.40 oil DIC M27 lens, zoom 3.0, and pinhole at 52 μm. The quantification of spine morphology (mature, stubby, and filopodia) was performed manually using "false" color images ZEN software as previously described (53, 54).

Organotypic slice homogenates and immunofluorometry

After sitagliptin treatment (100 μM, 11 days), two organotypic slices (4 confetti discs per slice) were pooled in 200 μl of Tris 10 mM/RIPA buffer (Tris 10 mM, pH 7.4, containing NaCl (150 mM), EDTA (1 mM), Triton X-100 (1%), deoxycholate (0.5%), and SDS (0.1%)). After 30 min in ice dry, confetti discs were removed and supernatants were mechanically homogenized by Potter. DPP4 activity was measured as described in DPP4 activity measurements (see below). For NeuN immunostaining, organotypic hippocampal slices were fixed with 4% of paraformaldehyde and then permeabilized overnight in PBS containing Triton X-100 (0.4%). Hippocampal slices were incubated in the saturation blocking buffer (PBS/Triton 0.1%-bovine serum albumin 5%) for 8 h and then hybridized with the anti-NeuN antibody (d:1/2500, Abcam, rabbit) in PBS/Triton 0.1% for 48 h. After three PBS washes, secondary antibodies were added overnight with 4′,6-diamidino-2-phenylindole (DAPI) in PBS/Triton 0.1%. Finally, slices were rinsed in double distilled water and then placed on the glass slide with the aqueous mounting medium. For pE3-xAβ immunostaining and before the permeabilization, organotypic hippocampal slices were included in paraffin with automatic tissue processor and then were deparaffined by three successive xylene baths (1 h per bath), two ethanol 100%, one ethanol 90%, and one ethanol 70% baths for 5 min. This sample preparation allowed unmasking with formic acid for 10 min. The pE3-xAβ antibody was diluted at 1/50 (IBL international) in PBS/Triton 0.1%.

Cytation imaging

Mouse neuroblastoma N2a cells (ATCC, CCL131) were grown in DMEM FCS (10%)-penicillin/streptomycin medium. Cells were plated in 6-well plates at a density of 100,000 cells/well. Five days after infection, cells were fixed for 20 min with paraformaldehyde (4%), washed three times with PBS, permeabilized for 5 min with Triton X-100 (0.1%), and blocked for 1 h with BSA (5%)/Tween (0.05%). The primary antibody against DPP4 (dilution of 1/500, Abcam ab28340) was added overnight, and then, cells were rinsed three times with PBS and incubated for 1 h with the secondary anti-goat antibody (Interchim, dilution of 1/500 + DAPI (1/20,000)). Cells were then rinsed again with PBS 1× and fixed with the VectaMount medium (Vector Laboratories) before Cytation imaging analysis with the Biotek Cytation 5 microscope, which automatically acquired six pictures per well with the same acquisition parameters (×20 magnification, numeric aperture 0.45, brightfield, at following excitation and emission wavelengths, respectively: DAPI (377; 447); GFP (469; 525); Texas Red (586; 647)). We used ImageJ software to quantify the fluorescence intensity Texas Red in GFP-positive cells.

DPP4 activity measurements

Hippocampi were homogenized in Tris buffer (10 mM, pH 7.5). DPP4 activity was measured in 50 μg of proteins, with or without the DPP4 inhibitor P32/98 (100 μM) using Gly-Pro–7-amido-4-methylcoumarin as the substrate (100 μM, Santa Cruz Biotech) in the assay buffer (Tris 50 mM, pH 7.5, a final volume of 100 μl). Fluorescence was recorded at 360-nm excitation and 460-nm emission wavelengths as described (50).

Animals

3xTg-AD (35) and 3xTg-WT (non transgenic) mice were generated from breeding pairs provided by Dr Franck LaFerla (Irvine). Animals were housed with a light/dark cycle (12 h:12 h) and were given free access to water and food. All experimental procedures were in accordance with the European Communities Council Directive of 22 September 2010 (2010/63/EU) and approved by the French Ministry of Higher Education and Research (Project number APAFIS#9645-2017012315473838) and by Côte d'Azur University Animal Care and Use Committee.

Viral production and stereotaxic injections

Lentiviral particles were produced as previously described (55). Viral titers were assessed using p24 ELISA (VPK-107; Cell Biolabs). Green, green-APPwt, and green-APPswe lentiviruses (cloned in the lentiviral vector with an IRES-ZsGreen fluorescent tag (pHAGE-CMV-MCS-IRES-ZsGreen)) (56) were under the control of the CMV promoter. shRNA constructs TCATCACCGTGCCAATAGTTCTGCTGAGC (shDPP4) and GCACTACCAGAGCTA ACTCAGATAGTT (shScr) were inserted in the vector pGFP-C-sh Lenti under the U6 promoter (Cat. No. T R30023, OriGene). Gene-specific mouse shRNA sequences are TL500553 CD26 (Gene ID 13482) Mouse shRNA under the U6 promoter. Two- to three-month-old WT and 3xTg-AD mice were anesthetized by intraperitoneal injection with a mixture of ketamine (100 mg/kg) and xylazine (10 mg/kg). Mice were bilaterally stereotaxically injected into the subiculum region (3 μl) with high titers of viral particles (1–1.5 × 10^{10} viral particles) at the following coordinates Sub: a/p: ± 3.8, m/l ± 2.5, d/v, −2.0 (The Mouse Brain in stereotaxic coordinates, Second Edition, *Elsevier* Academic Press).

In vivo *pharmacological treatments*

A selective and specific inhibitor of DPP4, sitagliptin (provided by Sigma-Aldrich, PHR1857.14) was administered once a day by intraperitoneal injections at a dose of 15 mg/kg (*i.e.*, 0.3 mg/day for a 20-g mouse) for a total of 6 weeks of treatment before animal sacrifices. To evaluate cerebral DPP4 activity, sitagliptin was administrated daily for 8 days and then DPP4 activity was measured as described above.

Barnes maze and MWM

For Barnes maze, spatial learning and memory were studied using a dry land–based rodent procedure (57). Mice performed during 3 to 4 days on a spatial acquisition protocol, allowing animals to retrieve a box placed under a hole of the Barnes maze apparatus, before being assessed for memory with a probe trial in which mice had a total time of 60 s to find the target place. Several parameters were evaluated including the

latency to reach the target site, number of quadrant crossing, latency, and distance in the quadrant of the target site.

MWM task was assessed in a circular pool filled with an opaque solution and placed in a room surrounded by visual clues. Maze was performed as previously extensively described (46). Data were analyzed with the ANY-maze 6.1 software.

Rotarod performance and open field tests

Locomotor performance of mice was tested on a rotarod apparatus (Bioseb, model LE8200) as previously described (46). Three trials were performed during a period of 5 min for each animal. Mice anxiety and exploratory behavior were recorded by an Open Field test. Briefly, time spent in the center of the box (40 × 40 cm) is recorded during 10 min per animal.

Immunohistochemistry

3xTg-WT or 3xTg-AD mice infected with lentiviruses or injected with pharmacological treatment were anesthetized as described. Mouse brains were embedded in paraffin and then sliced with a microtome apparatus at a thickness of 8 μm. Slices were treated with formic acid and then incubated overnight at 4 °C with a recombinant anti-beta amyloid 1 to 42 antibody that does not cross-react with Aβ37, 38, 40, and 43 (dilution 1/1000, H31L21, Invitrogen) or with anti-pEAβ antibody (dilution:1/50, rabbit, IBL international). After several washes, sections were incubated for 1 h with an anti-rabbit horseradish peroxidase. Slices were then revealed with the diaminobenzidine–ImmPACT system (Vector Laboratories).

Human brain sample preparation

Human brain samples were obtained from the "Neuro-CEB" Brain Bank. All procedures using human brain samples were performed in accordance with the ethical standards of both institutional and national research committees as well as the 1964 Helsinki declaration and amendments. In accordance with the French Bioethical Agreement (AC-2013-1887), individual consents were signed by the patients or their close relatives in their name. Cases were anonymized, and information regarding age, sex, and neuropathology is provided in Table S1. Tissue lysates were obtained after mechanical homogenization of temporal cortex sections. Powder was resuspended in Tris 10 mM, pH 7.5, and samples were mechanically homogenized by a Potter, sonicated, and analyzed for DPP4 enzymatic activity as described above.

Insoluble fraction preparations and Aβ quantitation by ELISA

Dissected hippocampi from 3xTg-WT and 3xTg-AD mice or organotypic hippocampal slices were homogenized in RIPA buffer containing a mix of protease inhibitors as previously described (58). Proteins were centrifuged after mechanical homogenization by a Potter (100,000*g*, 1 h, at 4 °C). Pellets containing insoluble material were resuspended in formic acid (70%), centrifuged (100,000*g*, 1 h, 4 °C), and then, supernatants were brought to pH 7.5 by addition of Tris HCl (1 M, pH 10.8) containing betaine (25 mM). This fraction was referred to as the insoluble fraction. Human Aβ40 and Aβ42 peptides levels were measured in insoluble fractions using sandwich enzyme-linked immunosorbent assay kits (BioSource, Invitrogen) as described (59).

Statistical analysis

Organotypic slices and MS were analyzed by one-way ANOVA and the Kruskal–Wallis ($^{*}p \leq 0.05$; $^{**}p < 0.01$; $^{****}p < 0.005$) test to study the spine morphology. DPP4 activities were compared by Wilcoxon ($^{*}p \leq 0.05$) and Mann–Whitney tests ($^{*}p \leq 0.05$). For behavioral experiments, all statistical analyses were realized using InVivoStat software. For each statistical analysis, normal distribution of residuals and homogeneity of variance were analyzed by checking normal probability plot and residual *versus* predicted plot. For Barnes maze and MWM task, escape latency was analyzed by mixed-model ANOVA with repeated measure (genotype x injection x training day) and followed by Benjamini–Hochberg's correction. Concerning statistics of probe phase MWM and Barnes maze, open field, and rotarod, the influences of both injection and genotype were considered by two-way ANOVAs (genotype and injection) with multiple comparisons adjusted by Benjamini–Hochberg's method. For open field statistical analyses, data were log-10–transformed to respect homoscedasticity assumptions. For immunohistochemistry, immunoprecipitation experiments, Aβ42-positive plaque number and morphology, and ELISA, we used the Mann–Whitney test. The number, area, and perimeter of plaques were analyzed by automatic-macro program on ImageJ software, and every point corresponds to an average of ten pictures for each mouse. The DPP4 activity in humans was performed using the two-way ANOVA test with Dunnett's multiple comparisons test.

Data availability

All data are contained within the article and in the accompanying supporting information.

Supporting information—This article contains supporting information.

Acknowledgments—The authors thank Dr La Ferla for initial supply of 3xTg-AD mice. This work was supported through the LABEX (excellence laboratory, program investment for the future) DISTALZ (Development of Innovative Strategies for a Transdisciplinary approach to ALZheimer's disease), the Hospital University Federation (FHU) OncoAge, and the Fondation Plan Alzheimer. The authors greatly thank Frédéric Brau and Sophie Abelanet at Imaging and Cytometry platform (Côte d'Azur, MICA). The authors thank Dr Luc Buée (UMR 837 Inserm-UDSL-CHRU, Centre de Recherche Jean-Pierre Aubert, Lille) for helpful discussions.

Author contributions—A. V., T. L., and F. C. formal analysis; A. V., T. L., D. D., A.-S. G., C. C., and M. C. investigation; A. V. methodology; A. V., J. D., M. C., and F. C. writing–review and editing; J.

D. and F. C. supervision; F. C. conceptualization; F. C. funding acquisition; F. C. writing–original draft; F. C. project administration.

Conflict of interest—The authors declare that they have no conflicts of interest with the contents of this article.

Abbreviations—The abbreviations used are: 3xTg-AD, triple transgenic AD; Aβ, amyloid β; AD, Alzheimer's disease; APA, aminopeptidase A; APP, amyloid precursor protein; APPswe, APP bearing the Swedish mutation; APPwt, wild-type APP; DAPI, 4′,6-diamidino-2-phenylindole; DPP4, dipeptidyl aminopeptidase 4; E3-Aβ, Glu3-Aβ; EBSS, Earles' Balanced Salt solution; FCS, fetal calf serum; flAβ, full-length Aβ; MWM, Morris water maze; pE3-Aβ, pyroGlu3–Aβ; QC, glutaminyl cyclase; shDPP4, shRNA probes targeting DPP4; shScr, shRNA corresponding to a control scramble sequence.

References

1. Hardy, J. A., and Higgins, G. A. (1992) Alzheimer's disease: The amyloid cascade hypothesis. *Science* **256**, 184–185
2. Checler, F. (1995) Processing of the b-amyloid precursor protein and its regulation in Alzheimer's disease. *J. Neurochem.* **65**, 1431–1444
3. Panza, F., Lozupone, M., Logroscino, G., and Imbimbo, B. P. (2019) A critical appraisal of amyloid-beta-targeting therapies for Alzheimer disease. *Nat. Rev. Neurol.* **15**, 73–88
4. Huang, Y. M., Shen, J., and Zhao, H. L. (2019) Major clinical trials failed the amyloid hypothesis of Alzheimer's disease. *J. Am. Geriatr. Soc.* **67**, 841–844
5. Herrup, K. (2015) The case for rejecting the amyloid cascade hypothesis. *Nat. Neurosci.* **18**, 794–799
6. Pulina, M. V., Hopkins, M., Haroutunian, V., Greengard, P., and Bustos, V. (2020) C99 selectively accumulates in vulnerable neurons in Alzheimer's disease. *Alzheimers Dement.* **16**, 273–282
7. Lauritzen, I., Pardossi-Piquard, R., Bourgeois, A., Pagnotta, S., Biferi, M. G., Barkats, M., Lacor, P., Klein, W., Bauer, C., and Checler, F. (2016) Intraneuronal aggregation of the beta-CTF fragment of APP (C99) induces Abeta-independent lysosomal-autophagic pathology. *Acta Neuropathol.* **132**, 257–276
8. Cavanagh, C., Colby-Milley, J., Bouvier, D., Farso, M., Chabot, J. G., Quirion, R., and Krantic, S. (2013) betaCTF-correlated burst of hippocampal TNFalpha occurs at a very early, pre-plaque stage in the TgCRND8 mouse model of Alzheimer's disease. *J. Alzheimers Dis.* **36**, 233–238
9. Mondragon-Rodriguez, S., Gu, N., Manseau, F., and Williams, S. (2018) Alzheimer's transgenic model is characterized by very early brain network alterations and beta-CTF fragment accumulation: Reversal by beta-secretase inhibition. *Front. Cell Neurosci.* **12**, 121
10. Kaur, G., Pawlik, M., Gandy, S. E., Ehrlich, M. E., Smiley, J. F., and Levy, E. (2017) Lysosomal dysfunction in the brain of a mouse model with intraneuronal accumulation of carboxyl terminal fragments of the amyloid precursor protein. *Mol. Psychiatry* **22**, 981–989
11. Lauritzen, I., Pardossi-Piquard, R., Bourgeois, A., Becot, A., and Checler, F. (2019) Does intraneuronal accumulation of carboxyl-terminal fragments of the amyloid precursor protein trigger early neurotoxicity in Alzheimer's disease? *Curr. Alzheimer Res.* **16**, 453–457
12. Shoji, M., Golde, T. E., Ghiso, J., Cheung, T. T., Estus, S., Shaffer, M., Cai, X. D., McKay, D. M., Tintner, R., Frangione, B., and Younkin, S. G. (1992) Production of the Alzheimer amyloid b protein by normal proteolytic processing. *Science* **258**, 126–129
13. Haass, C., Hung, A. Y., Schlossmacher, M. G., Oltersdorf, T., Teplow, D. B., and Selkoe, D. J. (1993) Normal cellular processing of the b-amyloid precursor protein results in the secretion of the amyloid b peptide and related molecules. *Nature* **695**, 109–116
14. Sevalle, J., Amoyel, A., Robert, P., Fournie-Zaluski, M. C., Roques, B., and Checler, F. (2009) Aminopeptidase A contributes to the N-terminal truncation of amyloid beta-peptide. *J. Neurochem.* **109**, 248–256
15. Castellani, R. J., Lee, H. G., Perry, G., and Smith, M. A. (2006) Antioxidant protection and neurodegenerative disease: The role of amyloid-beta and tau. *Am. J. Alzheimers Dis. Other Demen.* **21**, 126–130
16. Brothers, H. M., Gosztyla, M. L., and Robinson, S. R. (2018) The physiological roles of amyloid-beta peptide hint at new ways to treat Alzheimer's disease. *Front. Aging Neurosci.* **10**, 118
17. Dunys, J., Valverde, A., and Checler, F. (2018) Are N- and C-terminally truncated Abeta species key pathological triggers in Alzheimer's disease? *J. Biol. Chem.* **293**, 15419–15428
18. Schilling, S., Zeitschel, U., Hoffmann, T., Heiser, U., Francke, M., Kehlen, A., Holzer, M., Hutter-Paier, B., Prokesch, M., Windisch, M., Jagla, W., Schlenzig, D., Lindner, C., Rudolph, T., Reuter, G., *et al.* (2008) Glutaminyl cyclase inhibition attenuates pyroglutamate Abeta and Alzheimer's disease-like pathology. *Nat. Med.* **14**, 1106–1111
19. Cynis, H., Scheel, E., Saido, T. C., Schilling, S., and Demuth, H. U. (2008) Amyloidogenic processing of amyloid precursor protein: Evidence of a pivotal role of glutaminyl cyclase in generation of pyroglutamate-modified amyloid-beta. *Biochemistry* **47**, 7405–7413
20. Jawhar, S., Wirths, O., Schilling, S., Graubner, S., Demuth, H. U., and Bayer, T. A. (2011) Overexpression of glutaminyl cyclase, the enzyme responsible for pyroglutamate A{beta} formation, induces behavioral deficits, and glutaminyl cyclase knock-out rescues the behavioral phenotype in 5XFAD mice. *J. Biol. Chem.* **286**, 4454–4460
21. Rahfeld, J., Schutkowski, M., Faust, J., Neubert, K., Barth, A., and Heins, J. (1991) Extended investigation of the substrate specificity of dipeptidyl peptidase IV from pig kidney. *Biol. Chem. Hoppe Seyler* **372**, 313–318
22. Checler, F. (1993) Neuropeptide-degrading peptidases. In: Nagatsu, T., Parvez, H., Naoi, M., Parvez, S., eds. *Methods in Neurotransmitters and Neuropeptides Research. Part 2*, Elsevier Science Publishers, Amsterdam: 375–418
23. Antonyan, A., Schlenzig, D., Schilling, S., Naumann, M., Sharoyan, S., Mardanyan, S., and Demuth, H. U. (2018) Concerted action of dipeptidyl peptidase IV and glutaminyl cyclase results in formation of pyroglutamate-modified amyloid peptides *in vitro*. *Neurochem. Int.* **113**, 112–119
24. Angelopoulou, E., and Piperi, C. (2018) DPP-4 inhibitors: A promising therapeutic approach against Alzheimer's disease. *Ann. Transl. Med.* **6**, 255
25. Cheng, Q., Cheng, J., Cordato, D., and Gao, J. (2020) Can dipeptidyl peptidase-4 inhibitors treat cognitive disorders? *Pharmacol. Ther.* **212**, 107559
26. Barelli, H., Lebeau, A., Vizzavona, J., Delaere, P., Chevallier, N., Drouot, C., Marambaud, P., Ancolio, K., Buxbaum, J. D., Khorkova, O., Heroux, J., Sahasrabudhe, S., Martinez, J., Warter, J.-M., Mohr, M., *et al.* (1997) Characterization of new polyclonal antibodies specific for 40 and 42 aminoacid-long amyloid b peptides: Their use to examine the cell biology of presenilins and the immunohistochemistry of sporadic Alzheimer's disease and cerebral amyloid angiopathy cases. *Mol. Med.* **3**, 695–707
27. Miners, J. S., Baig, S., Palmer, J., Palmer, L. E., Kehoe, P. G., and Love, S. (2008) Abeta-degrading enzymes in Alzheimer's disease. *Brain Pathol.* **18**, 240–252
28. Nalivaeva, N. N., Belyaev, N. D., Zhuravin, I. A., and Turner, A. J. (2012) The Alzheimer's amyloid-degrading peptidase, neprilysin: Can we control it? *Int. J. Alzheimers Dis.* **2012**, 383796
29. Chen, H., Roques, B. P., and Fournie-Zaluski, M. C. (1999) Design of the first highly potent and selective aminopeptidase N (EC 3.4.11.2) inhibitor. *Bioorg. Med. Chem. Lett.* **9**, 1511–1516
30. David, C., Bischoff, L., Meudal, H., Mothe, A., De Mota, N., DaNascimento, S., Llorens-Cortes, C., Fournie-Zaluski, M. C., and Roques, B. P. (1999) Investigation of subsite preferences in aminopeptidase A (EC 3.4.11.7) led to the design of the first highly potent and selective inhibitors of this enzyme. *J. Med. Chem.* **42**, 5197–5211
31. Pospisilik, J. A., Stafford, S. G., Demuth, H. U., Brownsey, R., Parkhouse, W., Finegood, D. T., McIntosh, C. H., and Pederson, R. A. (2002) Long-term treatment with the dipeptidyl peptidase IV inhibitor P32/98 causes sustained improvements in glucose tolerance, insulin sensitivity, hyperinsulinemia, and beta-cell glucose responsiveness in VDF (fa/fa) Zucker rats. *Diabetes* **51**, 943–950

32. Green, B. D., Flatt, P. R., and Bailey, C. J. (2006) Dipeptidyl peptidase IV (DPP IV) inhibitors: A newly emerging drug class for the treatment of type 2 diabetes. *Diab. Vasc. Dis. Res.* **3**, 159–165
33. Valverde, A., Dunys, J., Lorivel, T., Debayle, D., Gay, A. S., Lacas-Gervais, S., Roques, B. P., Chami, M., and Checler, F. (2021) Aminopeptidase A contributes to biochemical, anatomical and cognitive defects in Alzheimer's disease (AD) mouse model and is increased at early stage in sporadic AD brain. *Acta Neuropathol.* **141**, 823–839
34. Dauch, P., Masuo, Y., Vincent, J. P., and Checler, F. (1993) A survey of the cerebral regionalization and ontogeny of eight exo- and endo- peptidases in murines. *Peptides* **14**, 593–599
35. Oddo, S., Caccamo, A., Shepherd, J. D., Murphy, G., Golde, T. E., Kayed, R., Metherate, R., Mattson, M. P., Akbari, Y., and LaFerla, F. (2003) Triple-transgenic model of Alzheimer's disease with plaques and tangles: Intracellular Ab and synaptic dysfunction. *Neuron* **39**, 409–421
36. Stover, K. R., Campbell, M. A., Van Winssen, C. M., and Brown, R. E. (2015) Early detection of cognitive deficits in the 3xTg-AD mouse model of Alzheimer's disease. *Behav. Brain Res.* **289**, 29–38
37. Portelius, E., Andreasson, U., Ringman, J. M., Buerger, K., Daborg, J., Buchhave, P., Hansson, O., Harmsen, A., Gustavsson, M. K., Hanse, E., Galasko, D., Hampel, H., Blennow, K., and Zetterberg, H. (2010) Distinct cerebrospinal fluid amyloid beta peptide signatures in sporadic and PSEN1 A431E-associated familial Alzheimer's disease. *Mol. Neurodegener.* **5**, 2
38. Yuan, X. Y., and Wang, X. G. (2017) Mild cognitive impairment in type 2 diabetes mellitus and related risk factors: A review. *Rev. Neurosci.* **28**, 715–723
39. Kosaraju, J., Holsinger, R. M. D., Guo, L., and Tam, K. Y. (2017) Linagliptin, a dipeptidyl peptidase-4 inhibitor, mitigates cognitive deficits and pathology in the 3xTg-AD mouse model of Alzheimer's disease. *Mol. Neurobiol.* **54**, 6074–6084
40. D'Amico, M., Di Filippo, C., Marfella, R., Abbatecola, A. M., Ferraraccio, F., Rossi, F., and Paolisso, G. (2010) Long-term inhibition of dipeptidyl peptidase-4 in Alzheimer's prone mice. *Exp. Gerontol.* **45**, 202–207
41. Chen, S., Zhou, M., Sun, J., Guo, A., Fernando, R. L., Chen, Y., Peng, P., Zhao, G., and Deng, Y. (2019) DPP-4 inhibitor improves learning and memory deficits and AD-like neurodegeneration by modulating the GLP-1 signaling. *Neuropharmacology* **157**, 107668
42. Gilbert, M. P., and Pratley, R. E. (2020) GLP-1 analogs and DPP-4 inhibitors in type 2 diabetes therapy: Review of head-to-head clinical trials. *Front. Endocrinol. (Lausanne)* **11**, 178
43. Kim, D. S., Choi, H. I., Wang, Y., Luo, Y., Hoffer, B. J., and Greig, N. H. (2017) A new treatment strategy for Parkinson's disease through the gut-brain axis: The glucagon-like peptide-1 receptor pathway. *Cell Transplant* **26**, 1560–1571
44. Nixon, R. A. (2017) Amyloid precursor protein and endosomal-lysosomal dysfunction in Alzheimer's disease: Inseparable partners in a multifactorial disease. *FASEB J.* **31**, 2729–2743
45. Goutagny, R., Gu, N., Cavanagh, C., Jackson, J., Chabot, J. G., Quirion, R., Krantic, S., and Williams, S. (2013) Alterations in hippocampal network oscillations and theta-gamma coupling arise before Abeta overproduction in a mouse model of Alzheimer's disease. *Eur. J. Neurosci.* **37**, 1896–1902
46. Bourgeois, A., Lauritzen, I., Lorivel, T., Bauer, C., Checler, F., and Pardossi-Piquard, R. (2018) Intraneuronal accumulation of C99 contributes to synaptic alterations, apathy-like behavior, and spatial learning deficits in 3xTgAD and 2xTgAD mice. *Neurobiol. Aging* **71**, 21–31
47. Wittnam, J. L., Portelius, E., Zetterberg, H., Gustavsson, M. K., Schilling, S., Koch, B., Demuth, H. U., Blennow, K., Wirths, O., and Bayer, T. A. (2012) Pyroglutamate amyloid beta (Abeta) aggravates behavioral deficits in transgenic amyloid mouse model for Alzheimer disease. *J. Biol. Chem.* **287**, 8154–8162
48. Bergman, A., Ebel, D., Liu, F., Stone, J., Wang, A., Zeng, W., Chen, L., Dilzer, S., Lasseter, K., Herman, G., Wagner, J., and Krishna, R. (2007) Absolute bioavailability of sitagliptin, an oral dipeptidyl peptidase-4 inhibitor, in healthy volunteers. *Biopharm. Drug Dispos.* **28**, 315–322
49. Bernstein, H. G., Dobrowolny, H., Keilhoff, G., and Steiner, J. (2018) Dipeptidyl peptidase IV, which probably plays important roles in Alzheimer disease (AD) pathology, is upregulated in AD brain neurons and associates with amyloid plaques. *Neurochem. Int.* **114**, 55–57
50. Ichai, C., Chevallier, N., Delaere, P., Dournaud, P., Epelbaum, J., Hauw, J. J., Vincent, J. P., and Checler, F. (1994) Influence of region-specific alterations of neuropeptidases content on the catabolic fates of neuropeptides in Alzheimer's disease. *J. Neurochem.* **62**, 645–655
51. Alexandru, A., Jagla, W., Graubner, S., Becker, A., Bauscher, C., Kohlmann, S., Sedlmeier, R., Raber, K. A., Cynis, H., Ronicke, R., Reymann, K. G., Petrasch-Parwez, E., Hartlage-Rubsamen, M., Waniek, A., Rossner, S., *et al.* (2011) Selective hippocampal neurodegeneration in transgenic mice expressing small amounts of truncated Abeta is induced by pyroglutamate-Abeta formation. *J. Neurosci.* **31**, 12790–12801
52. Miners, J. S., Barua, N., Kehoe, P. G., Gill, S., and Love, S. (2011) Abeta-degrading enzymes: Potential for treatment of Alzheimer disease. *J. Neuropathol. Exp. Neurol.* **70**, 944–959
53. Risher, W. C., Patel, S., Kim, I. H., Uezu, A., Bhagat, S., Wilton, D. K., Pilaz, L. J., Singh Alvarado, J., Calhan, O. Y., Silver, D. L., Stevens, B., Calakos, N., Soderling, S. H., and Eroglu, C. (2014) Astrocytes refine cortical connectivity at dendritic spines. *Elife* **3**, e04047
54. Qiao, H., Li, M. X., Xu, C., Chen, H. B., An, S. C., and Ma, X. M. (2016) Dendritic spines in depression: What we learned from animal models. *Neural Plast.* **2016**, 8056370
55. Cisse, M., Duplan, E., Lorivel, T., Dunys, J., Bauer, C., Meckler, X., Gerakis, Y., Lauritzen, I., and Checler, F. (2017) The transcription factor XBP1s restores hippocampal synaptic plasticity and memory by control of the Kalirin-7 pathway in Alzheimer model. *Mol. Psychiatry* **22**, 1562–1575
56. Bussiere, R., Lacampagne, A., Reiken, S., Liu, X., Scheuerman, V., Zalk, R., Martin, C., Checler, F., Marks, A. R., and Chami, M. (2017) Amyloid beta production is regulated by beta2-adrenergic signaling-mediated post-translational modifications of the ryanodine receptor. *J. Biol. Chem.* **292**, 10153–10168
57. Lena, I., and Mantegazza, M. (2019) NaV1.2 haploinsufficiency in Scn2a knock-out mice causes an autistic-like phenotype attenuated with age. *Sci. Rep.* **9**, 12886
58. Pardossi-Piquard, R., Lauritzen, I., Bauer, C., Sacco, G., Robert, P., and Checler, F. (2016) Influence of genetic background on apathy-like behavior in triple transgenic AD mice. *Curr. Alzheimer Res.* **13**, 942–949
59. Lauritzen, I., Pardossi-Piquard, R., Bauer, C., Brigham, E., Abraham, J. D., Ranaldi, S., Fraser, P., St-George-Hyslop, P., Le Thuc, O., Espin, V., Chami, L., Dunys, J., and Checler, F. (2012) The beta-secretase-derived C-terminal fragment of betaAPP, C99, but not Abeta, is a key contributor to early intraneuronal lesions in triple-transgenic mouse hippocampus. *J. Neurosci.* **32**, 16243, 1655a